

Metrological Measurements Using Programmable Josephson Voltage Standard

Tezgül COŞKUN ÖZTÜRK^{1,2}, Sarp ERTÜRK², Ali TANGEL², Mehedin ARİFOVIÇ¹, Saliha TURHAN¹

¹TÜBİTAK Ulusal Metroloji Enstitüsü, TÜBİTAK Gebze Yerleşkesi, Gebze/Kocaeli, Türkiye
tezgul.ozturk@tubitak.gov.tr, mehedin.arifovic@tubitak.gov.tr

²Kocaeli Üniversitesi, Müh. Fakültesi, Elektronik ve Haberleşme Müh., Umuttepe Yerleşkesi, İzmit/Kocaeli Türkiye

Abstract

In this study, Programmable Josephson Voltage Standard established in UME is used in static and dynamic ADC characterization, and solid state voltage standard calibration. Model functions of the measurements are created including the stray components in the measurement circuit. Uncertainties of the measurements are evaluated according to the model functions. Software tools and mathematical tools for investigating the quantum state of the measurements are presented. Gain difference between the static and dynamic gain parameters is suggested to be used for digital metrology.

1. Introduction

In 1962 Brian Josephson predicted the intrinsic behavior of the Cooper pairs when they are tunneled through a thin barrier of insulator installed between two superconductors [1] and in 1963 his theory is proved [2,3]. After these dates many experiments [4] are performed to prove the frequency-voltage relation which is given in Equation 1. Several experiments have shown that the equation is independent from geometry and material of the junction, power of the microwave and magnetic field [4]. In this equation V_J is the voltage across the barrier when the superconducting Josephson Junction (JJ) is biased with appropriate dc and ac currents as illustrated in Figure 1. f is the frequency of the ac current applied through the junction, h and e are the Planck and the electron charge constants respectively and n is an integer. The presence of such an equation promises the voltage agreement at the accuracy and stability of the frequency.

$$V_J = n \cdot f \cdot h / 2e \quad (1)$$

The experimental proof of this equation encouraged metrologists to measure $2e/h$ known as the Josephson constant (K_J). The present value of K_J is accepted in 1990 and denoted with K_{J-90} after a comparison which has 0.4 ppm uncertainty [6,7]. Accepting a conventional value for K_{J-90} improved the voltage unit Volt firstly to 0.01 ppm level with single JJ and to 0.001 ppm level with arrays of JJs [5]. Connecting the JJs serially has been possible in 1981 using underdamped JJs because of the lack of JJs with the same electrical attributes. With underdamped JJs it is possible to generate V_J , while the dc current is zero for all voltage steps, for $n=0, \pm 1, \pm 2, \pm 3$ [8]. These dc zero current crossing voltage steps were enabling technology for Josephson Voltage Standards (JVS) and mostly called Conventional JVS while they had intrinsic and unwanted two disadvantages: 1- Changing rapidly between different steps was not possible and 2- noise sometimes could change the steps randomly [5].

In 1995 another kind of JVS that has voltage steps which are stable and programmable by changing the dc current, called Programmable JVS (PJVS) is suggested [5]. In this standard JJs are over-damped and n is 0 or ± 1 . Different quantum voltages are

selected by changing the dc current of the arrays of JJs as illustrated in Fig.1. This standard over-comes the two disadvantages of the Conventional JVSs and more over enables the dynamic measurements of DAC&ADCs at low frequencies. Rapid changing from one step to another is allowing synthesis of stepwise approximated AC signals so that PJVSs became the basis for electrical metrology at low frequencies [10] especially for digital metrology aspects.

In this study established PJVS standard is briefly introduced. With the measurements in Sections 3.1 and 3.2 the quantum state of the standard is presented. With the measurements in Section 3.3 the traceability to quantum standard for dynamic ADC characterization is presented. This ADC will be used in resistive voltage divider characterization in the QuADC [11] project.

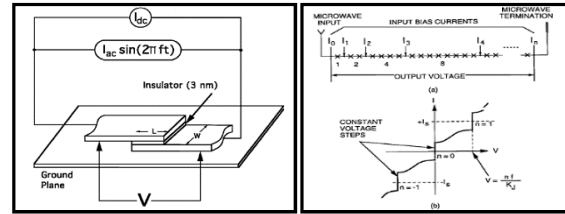


Fig.1 Biasing Josephson Junctions [5]

2. Components of the System

The heart of PJVS is the Superconducting Integrated Circuit (SIC) consisting of over-damped JJs and distributed microwave architecture [9]. The integrated circuit is borrowed from PTB within cooperation in Q-Wave and QuADC [11] projects. The integrated circuit has Nb as a superconductor. The temperature of superconductivity of Nb is 9.2 K. The temperature environment below 9.2 K is provided by liquid helium in a dewar. The integrated circuit on a carrier shown in Fig. 2 is immersed in a liquid helium, via a so-called cryoprop. The task of the cryoprop is to transmit microwaves and \pm In currents shown in Fig.1, as well as immersing the chip in liquid helium. To lock the phase of the microwave source and thus increase the frequency accuracy, a high-stability rubidium or cesium oscillator is used. The dc currents are provided by bias electronics consisting of synchronized DACs as shown in Fig.1. The PJVS voltage needs to be "floating": For this reason, the synchronization signals must be converted to optical signals through the optical "transmitter" and then to the electrical signal again via the optical "receiver". This process is carried out with an optical transceiver system. In addition, the system consists of a 28-bit multimeter (voltmeter, ADC) that checks whether or not the generated voltages are at quantum accuracy, a computer and software that calculates the DAC voltage and loads the voltage information into the DACs and receives and evaluates the ADCs measurement data. The system is shown in Figure 2 .

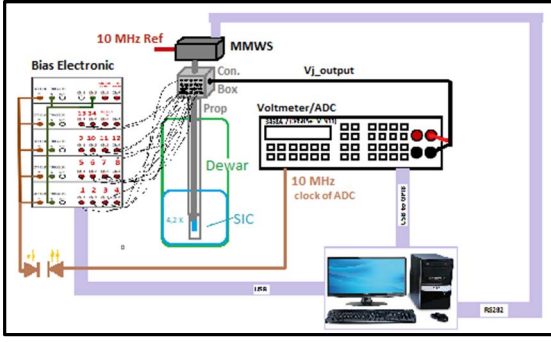


Fig.2 Established PJVS System

3. Metrological Measurements

3.1 Static ADC Characterization:

The system is ready to use after the probe is submerged in liquid helium, and the I_{n_ideal} currents the center currents of steps in the I-V curves shown in Fig.1 are measured. Whether the voltage output is at quantum level for all steps shown in Fig.3 can be checked using the voltmeter in the system. Within this control, the ADC / voltmeter is also statically characterized.

The integration time for static calibration was chosen as 20 NPLC (Number of Power Line Cycles), that means 400 ms. In Figure 4-a, the graph on the left shows a 64-step triangular wave applied by PJVS and measured by the ADC. In Fig. 4 a) the plot on the right $I_{segtrim}$ versus ADC measurements are shown. The difference of the bias current from the I_{n_ideal} currents is denoted $I_{segtrim}$. In many articles [12], the difference current from the I_{n_ideal} currents is called "Bias trimcurrent" while in some articles it is called dithering current. The program has two additional parameters for the *iteration* of the ($I_{segtrim}$) currents. These parameters are the number of iterations and the iteration step ($I_{iteration}$). Before calculating the V_n voltages the output voltages of the DACs, the I_{n_ideal} currents for each iteration are recalculated by using the Equation 2:

$$I_{n_ideal_new} = I_{n_ideal} - \left(\frac{iteration\ number}{2} \cdot iteration \cdot I_{iteration} \right) \quad (2)$$

$I_{segtrim}$ currents are measured by using Equation 3.

$$I_{segtrim} = \frac{V_n - V_{ADC}}{R_n} - I_{n_ideal} \quad (3)$$

If the voltmeter behaves linear and PJVS applies quantum voltages, the difference signal ($V_{quantum} - V_{3458}$) should follow the envelope shown in Fig.4 a). In addition, the difference between the $I_{segtrim}$ currents, belonging to one period, measured in the diagram of the $I_{segtrim}$ must be smaller than the μA . In other words, all measurement results must be within predetermined trends. To examine this difference, Fig. 4-b) and c) is shown when the difference button is pressed. Fig. 4. b) shows that the measurement results are at quantum quantum level. However, some steps in Figure 4 c) appear to be non quantum.

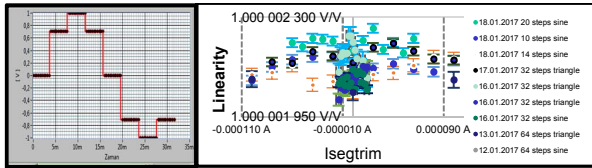


Fig.3 Generating Arbitrary Quantum Voltages with different $I_{segtrim}$ Settings, Measured Gain Dependent on $I_{segtrim}$ and shape of quantum voltages

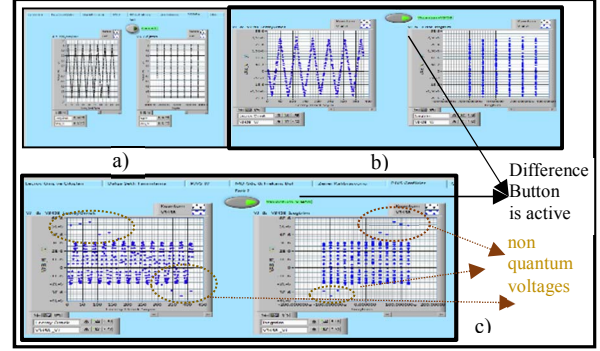


Fig.4. User interface for evaluating the quantum state of the measurements

In other words linearity of the ADC, can be observed from the difference signal ($V_{quantum} - V_{3458}$). With this interface, it is possible to check whether there is a problem in the system during the measurement and observe whether the flux is trapped or not. In Fig.3, the gains of the fitted linear curves for each period are given for varying $I_{segtrim}$ currents and waveforms. The lack of correlation between changing $I_{segtrim}$ and the gain indicates that the PJVS system works correctly, at quantum level. Gain measurement obtained with one waveform depending on different $I_{segtrim}$ s for each period are given in Fig.5. The R^2 parameter shown on the Fig.5 is the measurement of correlation. If the correlation is strong R^2 equals to 1. The existence of correlation between $I_{segtrim}$ currents and the gain can be tested by hypothesis testing using the Equation 4. In this equation $R^2 = r^2$, t_{meas} is the measured t distribution and $t_{12;0.05}$ coefficient from t distribution table, that is for 12 measurement number (n) for %95 probability.

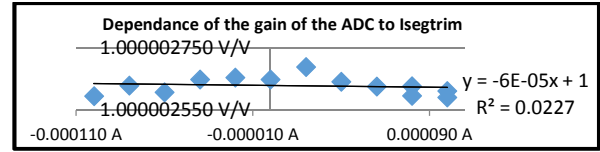


Fig.5. Dependence of the gain of the ADC to $I_{segtrim}$

$$t_{meas} = \frac{r}{\sqrt{\frac{1-r^2}{n-2}}} = \frac{\sqrt{0,0227}}{\sqrt{\frac{1-0,0227}{12-2}}} \approx 0,5 < t_{12;0,05} = 1,771 \quad (4)$$

As a consequence the effect of the slope measured in Fig.5 is negligible and the instability of the measured gain is due to measurement itself but not the PJVS. The voltmeter gain's type A uncertainty given in Fig.3 is at most 35 (nV/V)/(V/V) (coverage factor of 95%). In order to better estimate uncertainties coming from the measurement setup, measurement circuit is given in Fig.6 including all the stray components. Using circuit analysis theorems it is found that the measured voltage is dependent to the circuit elements as defined in Equation 5. $V_{thermal}$ voltage shown on the Fig.6 is due to the big temperature difference between the 4.2 K liquid helium and room environment which is around 300 K. The See-back effect, which occurs when different metals are connected is the reason of such a big thermal voltage difference this effect is eliminated by measuring the offset of the setup while V_j is set to 0 V that means all the junctions are in 0 Shapiro state. The actual result is the difference between the two measurements. ϵ_{DMM} in Equation 5 is the voltmeter's noise. Equation 6 is the model function of the measurement based on the error of the ADC which is the difference of V_{UUT_i} indicated value and V_{UUT_DMM} applied value.

Here $V_{UUT_i,0}$ is the measurement obtained with the ADC while V_J is 0 V. The $m_{I_{segtrim}}$ given in Equation 6 is the slope defining the existence of $I_{segtrim}$ dependence. If the correlation is tested as in Equation 4, and if the test is false than $m_{I_{segtrim}}$ is equal to 0. The $\delta V_{thermal}$ and δI_{offset} given in Equation 6 are the difference between the two measurements for $V_J=0$ and at the absolute voltage. It is clear that if the time between the two sequential measurements is short measurement uncertainty is only effected by the short time stability of Unit Under Teste (UUT) and the input resistance of UUT dependent with the R_{cable_prop} resistance of the prop.

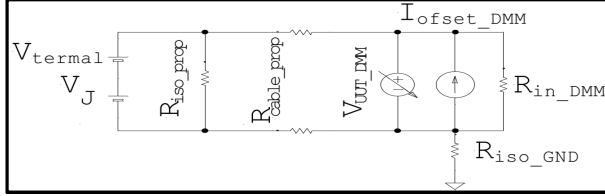


Fig.6. Measurement circuit of static ADC characterization

$$V_{UUT_{DMM}} = V_J \frac{R_{in_{DMM}}}{R_{cable_prop} + R_{in_{DMM}}} + V_{thermal} \frac{R_{in_{DMM}}}{R_{cable_prop} + R_{in_{DMM}}} + I_{offset} \frac{R_{in_{DMM}} R_{cable_prop}}{R_{cable_prop} + R_{in_{DMM}}} + \epsilon_{DMM} \quad (5)$$

$$\Delta E = V_{UUT_i} - V_{UUT_{i,0}} - \left\{ V_J \frac{R_{in_{DMM}}}{R_{cable_prop} + R_{in_{DMM}}} + \delta V_{thermal} \frac{R_{in_{DMM}}}{R_{cable_prop} + R_{in_{DMM}}} + \delta I_{offset} \frac{R_{in_{DMM}} R_{cable_prop}}{R_{cable_prop} + R_{in_{DMM}}} + m_{I_{segtrim}} \cdot I_{segtrim} \right\} \quad (6)$$

Also when the ADC gain m is found by fitting the measurement results as in Equation 7, the uncertainty of the gain is less dependent on the circuit parameters: k is the number of steps of the waveform shown in Fig.3, m is the gain of the ADC and n is the offset of the fitted linear curve. For easiness $V_{UUT_{DMM}} = V_R$; $V_{UUT_i} = V_i$ can be denoted. Equation 8 is the definition of the gain using least square error method for fitting. As can be easily seen from the Equation 10 the measured gain is less dependent to circuit parameters.

$$V_{UUT_i}[k] = m \cdot V_{UUT_{DMM}}[k] + n \quad (7)$$

$$m = \frac{\sum_{n=1}^N (V_R[k] - \bar{V}_R) \cdot (V_i[k] - \bar{V}_i)}{\sum_{n=1}^N (V_R[k] - \bar{V}_R)^2} \quad (8)$$

$$V_R[k] - \bar{V}_R = K \cdot V_J[k] + K \cdot \bar{V}_J + K \cdot \delta V_{thermal} + K \cdot \delta I_{offset} \cdot R_{cable_prop};$$

$$K = \frac{R_{in_{DMM}}}{R_{in_{DMM}} + R_{cable_prop}} \quad (9)$$

$$m = \frac{K \sum_{n=1}^N (V_J[k] - \bar{V}_J + \delta V_{thermal} + \delta I_{offset} \cdot R_{cable_prop}) \cdot (V_i[k] - \bar{V}_i)}{K \sum_{n=1}^N (V_J[k] - \bar{V}_J + \delta V_{thermal} + \delta I_{offset} \cdot R_{cable_prop})^2} \quad (10)$$

The static characterization of the ADC is done by fitting the gain for one period. If the number of quantum steps in a period are less, due to short time between the samples $\delta V_{thermal}$ and δI_{offset} are closing to zero. The step number in a period is changed and 4, 8, 10, 20 and 100 sampled waves are used for gain estimation. Type A uncertainty is better for 4-20 stepped samples compared to 100 samples per period. Voltmeter using integrating ADC is

characterized by 64-step, 32-step, 20-step, 10-step and 8-step sine and triangle waveforms. The gain of the voltmeter was not affected by the number of steps and waveform of the input. The Integral NonLinearity (INL) error of an ADC is defined as the maximum deviation from the fitted linear curve of the measurement results obtained with the ADC, divided to the used range of the ADC. The INL errors for each period are distributed as shown in Fig.7. The INL error is found for the voltmeter for the 1 V measurement range and it is within the INL error declared in [4] (<0.12 ppm) even for 1 V range as shown in Fig.7.

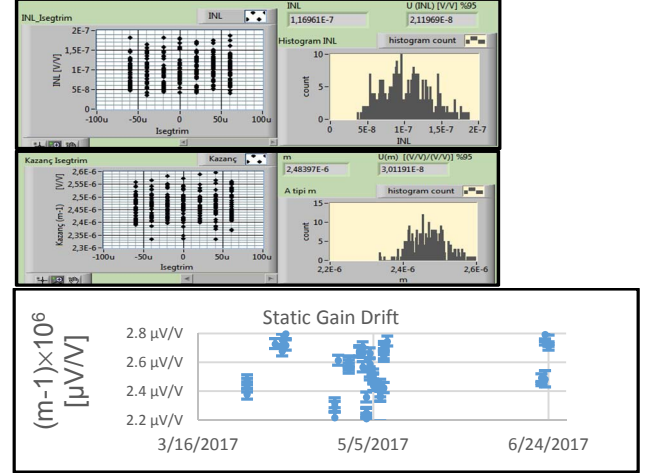


Fig.7. Drift of the static gain of the ADC & Histograms of the measured gain and INL

3.2 Solid State Voltage Standard (SSVS) Calibration:

In TUBITAK UME, SSVSs are traceable to Conventional JVSs. The comparison of the installed PJVS system with the another Josephson system rather than directly, using the SSVS as a transfer standard is preferred. For this reason, superconducting and solid state standards are interconnected on a thermal block as shown in Figure 8. The thermal block acts as a switch made of copper shown in brown color in Fig.8. Copper is preferred because of its high temperature conductivity. The reason for the large mass of the copper block being about 3 cm in thickness is to prevent sudden temperature changes. The semiconductor voltage standard shown by the V_{UUT} symbol, in Fig.8, is reversed again through the shorts made of copper. The reversal of the quantum voltage indicated by the symbol V_J is realized by changing the I_{ideal} currents by the program.

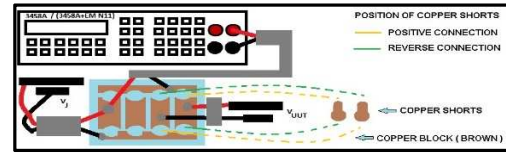


Fig.8 Comparison of the PJVS and SSVS

The voltmeter integration time for this measurement is set to 20 NPLC. The 20-sample symmetric square wave is produced whose amplitude is quantized to the last calibration value of the SSVS. The purpose of this is to reduce the uncertainty of the voltmeter gain by reducing the difference voltage between the two voltage standards to a minimum. The low potentials (black wires) of the two standards are short-circuited with one of the shorts on the block. The other short was used to short-circuit the

low potential of the voltmeter with the high potential of the V_{UUT} . This measurement can be modeled mathematically with Equation.11. The V_{DVM} is the reading of the voltmeter and it consist of the actual difference V_{diff} , thermal voltages in the setup and offset voltages denoted with V_{offset} of the DVM. The aim of the reversing, is to eliminate the thermal voltage offsets due to huge temperature difference and offset currents of the null detector. The reverse measurement can be modeled with Equation 12. All the process is explained mathematically in Equations 11-13. The rapid change of the symmetrical square wave with a positive and negative potential is superior to the Conventional JVSs so that the measurement results are not influenced by the offset of the measurement (V_{offset}) and the thermal voltage ($V_{thermal}$) changes.

$$V_{UUT}^+ = V_J^+ - V_{DVM}^+ = V_J^+ - V_{diff} - V_{thermal} - V_{offset} \quad (11)$$

$$V_{UUT}^- = V_J^- - V_{DVM}^- = V_J^- + V_{diff} - V_{thermal} - V_{offset} \quad (12)$$

$$V_{UUT} = \frac{V_{UUT}^+ - V_{UUT}^-}{2} = \frac{V_J^+ - V_J^- - 2 \times V_{diff} + \delta V_{thermal} + \delta V_{offset}}{2}; \quad (13)$$

$$V_J^+ = -V_J^-; \quad \delta V_{thermal}, \quad \delta V_{offset}: \text{voltage drifts}$$

In order to better evaluate all the effects due to stray components the measurement setup on more detail is given in Fig.9. Such an analysis can clarify in more detail the uncertainty budget given in [4]. Using the superposition circuit theory in the two circuits shown in Fig. 9, we can rewrite the equations (11) - (13) given above as in (14). The uncertainties given in [4] apply to the case where Conventional JVS is used. However, when PJVS is used, in addition to these components, the current dependence of the measurement result should also be assessed. For this reason, the current dependence parameter is measured as shown in Fig.10 by changing the I_{segrim} . Using Equation 4 for measurement given in Fig. 10, can be shown that there is not I_{segrim} dependence. A more comprehensive model function including the noises of SSVSs and the voltmeter can be rewritten as in Equation 14. The symbols used in the equation are defined in Table 1, uncertainty convenient to Guide of Expression of Uncertainty (GUM)[13] is evaluated in Table 2.

$$V_{UUT} = \frac{V_{UUT}^+ - V_{UUT}^-}{2} = \left\{ \frac{n \cdot N \cdot f}{K_{J90}} + \delta V_{thermal} \right\} \cdot \frac{R_{in_DMM} + R_{in_UUT}}{R_{in_DMM} + R_{in_UUT} + R_{cable_prop}} + (-V_{diff} + \epsilon_{DVM}) \cdot \frac{R_{in_DMM}}{R_{in_DMM} + R_{in_UUT}} + \delta I_{offset} \cdot (R_{cable_prop} + R_{in_UUT}) + \epsilon_{zener} + m_{I_{segrim}} \cdot I_{segrim} \quad (14)$$

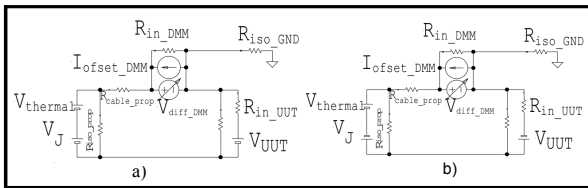


Fig.9 Electrical circuit of SSVS measurement setup

The difference from the nominal value of 1.018 V of SSVS (with serial number of 5610310) dependent to time is given in Figure 11.

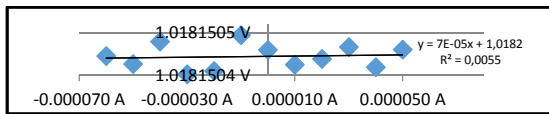


Fig.10 I_{segrim} dependence of the SSVS measurement result

As seen from this figure, the stability of the standard in a period of 10 days is examined and each measurement result is shown with blue marker. The time between the result of the comparison in Fig.11 with the red marker (comparison with PJVS) and green (comparison with Conventional JVS) is approximately one week. The graph shows that the measurement results are within the periodic short-term stability of the device.

Table.1 Symbols used in Equation 14

Josephson Constant	K_{J90}
Number of junctions on $\pm I$. Shapiro	N
Shapiro number: 0,1, -1	n
Microwave Frequency	f
Difference measured with DVM	V_{diff}
Thermal Voltage difference (@30 s)	$\delta V_{thermal}$
Offset Current drifts of the voltmeter (@30 s)	δI_{offset}
Input resistance of the voltmeter	R_{in_DMM}
Isolation resistance of the cable used to connect the voltmeter	$R_{iso_DMM_cable}$
Input resistor of the SSVS	R_{in_UUT}
Noise of the SSVS	ϵ_{zener}
Noise of the Digital Voltmeter (Bant Width 0.25 Hz)	ϵ_{DVM}
Difference of each channel's current from I_{ideal} current	I_{segrim}
Slope of the measurement result I_{segrim} dependence	$m_{I_{segrim}}$
Measurement Result	V_{UUT}

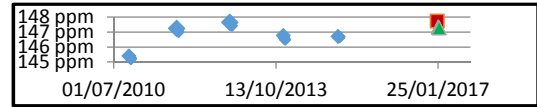


Fig.11. Comparison of the measurement results

Table 2. Uncertainty evaluation of SSVS calibration

	X_i	$u(X_i)$	$u(y)$
K_{J90}	483597,90 GHz/V		
N	7034		
n	1		
f	70,00000000 GHz	$< 0,000000010$ GHz	$< 0,1$ nV
V_{diff}	9481 nV	$< 0,2$ nV	$< 0,2$ nV
$\delta V_{thermal}$	0 nV	$< 0,1$ nV	$< 0,1$ nV
δI_{offset}	0,00000 nA	$< 0,015$ nA	$< 15,0$ nV
R_{in_DMM}	> 10 G Ω	> 10 G Ω	$< 0,0$ nV
$R_{iso_DMM_cable}$	> 1000 G Ω	> 1000 G Ω	$< 0,0$ nV
R_{in_UUT}	~ 1000 Ω		$< 0,0$ nV
R_{cable_prop}	~ 8 Ω		$< 0,0$ nV
ϵ_{zener}	0 nV	$< 6,0$ nV	$< 6,0$ nV
ϵ_{DVM}	0 nV	$< 2,0$ nV	$< 2,0$ nV
I_{segrim}	0,00000 nA	$< 120,0$ μ A	$< 0,0$ nV
$m_{I_{segrim}}$	0,00000 V/A	0,0000 V/A	$< 0,0$ nV
V_{UUT}	1,018150441 V	(1 σ)	$< 16,3$ nV
		(2 σ)	$< 32,6$ nV
		(2 σ)	$< 32,0$ nV/V

Type A uncertainty of the measurements given in Fig.10 is calculated to be around 10 nV (1 σ). This uncertainty is a bit more than total uncertainty given in [4]. The reason of this difference is investigated: I_{offset} stability of the digital voltmeter is measured using a 1 k Ω resistor by taking average for ten measurements and subtracting each successive 10 measurements in between. The result is divided to 1 k Ω and the offset current stability is found to be about ~ 0.015 nA. Additionally the nanovoltmeter bandwidth is a bit more than given in [4]. Taking into account the bandwidth and the input resistor of the measurement circuit the given uncertainty due to the noise of the

DVM is estimated to be bigger than that of at [4]. The SSVS noise is assumed to be the same as in [4]. Any gain correction is not applied so the uncertainty of V_{diff} is assumed to be $20 \mu\text{V/V}$. Better uncertainty can be obtained using nanovoltmeters as EM N11 or Keithley 2182/ HP34420 as might be used in [4] still obtained uncertainty is sufficient because it is less than weekly stability of the SSVS.

3.3 Dynamic IADC Characterization

Classic AC metrology based on using thermal converters does not meet the demand of recently developed digital metrology. The heart of digital metrology is ADC. Integrating ADC (IADC) is most commonly used ADC in metrology. PJVS standard is used to investigate how the ADC gain changes depending on the dynamic conditions in which the input signal changes rapidly and the integration period decreases while the sampling frequency increases. In Figure 2, the generation of the quantum signal is synchronized with the 10 MHz clock of the ADC. This synchronization is important so that non-quantum measurements during the transition from one step to another are subtracted from the measurement results. Before each dynamic gain measurement the static gain of the IADC is calibrated as explained in section 3.1 of this article. It is investigated many times as demonstrated in Fig.3 that 4 sampled and more than 4 sampled sine waves gives the same gain results for the IADC. The difference of dynamic gain from static gain (Δm) can be used for correction and stability in the ADC measurements. Level triggering and external triggering is used to start the measurement. There is not any significant change in between. For simplicity in most of the measurements, level of the input signal is used for triggering the measurement. The latency is declared to be around 700 ns in [14] which does not affect measurement where the sampling frequency (f_s) is less than 20 kHz. Delay of suitable time which is a multiple of 100 ns, is introduced after triggering to ensure that the measurements are on step. After delay, one measurement per step is obtained. The parameters of dynamic measurements: measurement frequency (f_m), integration time (T_i), waveform type, sampling frequency (f_s) are selected according to following criteria: The divider in the QuADC [11] project will be investigated according to sinusoids so sine forms are selected. To understand the effect of sampling frequency step number is changed between 8 and 128. The frequency of the signal is changed from 1 Hz to 400 Hz. The integration time is selected to cover the three ranges of T_i given in Fig.12 and previously used T_i parameters in the Q-Wave comparison [15]. Evaluating the gain using linear fitting or RMS calculation is possible and gives the same results. For stepped input signal as shown in Fig.3, it is not necessary to correct the transfer function of the integrating ADC. In Fig.13 the measured gain difference is given for some of the measurements. Up to 400 Hz such an analysis is made.

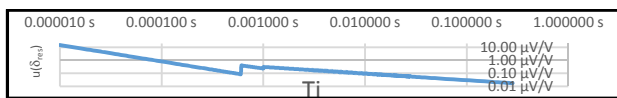


Fig.12 Resolution relative to the range of ADC dependent on T_i [16]

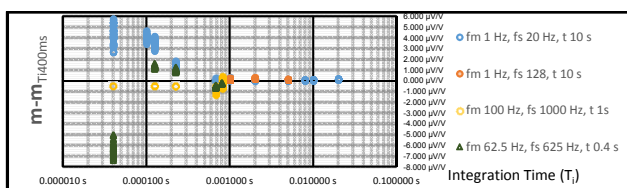


Fig.13 Measured gain difference according to T_i and f_s

4. Conclusions

In this study, Programmable Josephson Voltage Standard established in UME was used in static and dynamic ADC characterization and SSVS calibration. Model functions of the measurements were created including the stray components in the measurement circuit. Uncertainties of the measurements were evaluated according to the model functions. Software and mathematical tools for investigating the quantum state of the measurements were presented. The studies presented in Sections 3.1 and 3.2 has shown that the system is able to calibrate static and dynamic gains of the high precision ADCs/DACs. In Section 3.3 the gain difference parameter which is the difference between the static and dynamic gain was measured and suggested to be used in digital metrology. This parameter can be used to establish traceability of dynamic measurements to quantum standards. Measurements presented in Fig.13 bring out that uncertainties of RMS measurements of sinewaves by sampling techniques for frequencies less than 100 Hz can be lowered down to sub ppm level, already declared by UME as $5 \mu\text{V/V}$ at [15]. Analyzing the gain according spectral techniques is being investigated using the measurement data and detailed article on dynamic IADC characterization is being prepared.

5. Acknowledgements

This work is partly carried out with funding by the EA within the EMPIR JRP QuADC. The EMPIR is jointly funded by EMPIR participating countries and EURAMET. T.C.Ö. wants to thank Ralf Behr from PTB for valuable discussions on Josephson Voltage Standard Systems and borrowing the SIC.

5. References

- [1] B.D.Josephson, "Possible New Effects in Superconductive Tunneling", Phys. Letters, pp. 251-253, 1962
- [2] Anderson P., R. J. M., "Probable Observation of the Josephson Superconducting Effect". Phys. Rev. Lett, vol 10, pp. 230-232, 1963
- [3] S.Shapiro, "Josephson Currents in Superconducting Tunneling: The Effect of Microwaves and Other Observations", Phys. Letters, vol. 11, num 2, pp 80-82, July,1963.
- [4] P Pöpel, R., "The Josephson Effect and Voltage Standards" Metrologia, vol 29, pp. 153-174, 1992.
- [5] Samuel P. Benz, C. A. H., "Application of the Josephson Effect to Voltage Metrology". Proceedings of the IEEE, vol. 92, no. 10, 2004.
- [6] V. Sienknecht and T. Funck, "Realization of the SI Unit Volt by Means of a Voltage Balance", Metrologia 22,209-212, 1986
- [7] Taylor B. N., W. T. J., Metrologia, Issue 26, pp. , 1989
- [8] Kautz R. L., "On a proposed effect voltage standard at zero current bias" Appl. Phys. Lett., Issue 36, pp. 386-388, 1980.
- [9] F.Mueller, R. Behr, T.Weimann, L. Palafox, D. Olaya, P. D.Dresselhaus, and S.P.Benz, "1V and 10VSNS programmable voltage standards for 70GHz,"IEEE Trans. Appl. Supercond., vol. 19, no. 3, pp. 981-986, Jun. 2009
- [10] Ralf Behr, O. K. J. K. F. M. a. L. P., "Development and metrological applications of Josephson arrays at PTB". Meas. Sci. Technol. Issue 23, 2012.
- [11] <https://www.ptb.de/empir/quadc-project.html>
- [12] Seron, O. at all, "Precision ac-dc transfer measurements with a Josephson waveform synthesizer and a buffer amplifier." IEEE Trans. Instrum. Meas. , Issue 61, p. 198-204, 2012
- [13] "Guide to the Expression of Uncertainty in Measurement", GUM,1995
- [14] Agilent Technologies, 2001. "3458A Multimeter Calibration Manual". U.S.A.: Agilent Technologies
- [15] Nissila, J. and at all, "Stable Arbitrary Waveform Generator as a Transfer Standard for ADC Calibration" Conf. on Prec. Electromagnetic Meas, (CPEM 2016) Ottawa, 10-15.07.2016,
- [16] Ihlenfeld, K. W. G., 2001. Maintenance and traceability of AC voltages by synchronous digital synthesis and sampling, Braunschweig, Germany: PTB Report E-75